Large magnetic cooling power involving frustrated antiferromagnetic spin-glass state in R_2NiSi$_3$ (R = Gd,Er)

Santanu Pakhira,[1] Chandan Mazumdar,[1] R. Ranganathan,[1] S. Giri,[2] and Maxim Avdeev[3,4]

[1]*Condensed Matter Physics Division, Saha Institute of Nuclear Physics, 1/AF, Bidhannagar, Kolkata 700064, India*
[2]*Department of Solid State Physics, Indian Association for the Cultivation of Science, Jadavpur, Kolkata 700032, India*
[3]*Australian Nuclear Science and Technology Organisation, Locked Bag 2001, Kirrawee DC, NSW 2232, Australia*
[4]*School of Chemistry, The University of Sydney, Sydney, NSW 2006, Australia*

The ternary intermetallic compounds Gd$_2$NiSi$_3$ and Er$_2$NiSi$_3$ are synthesized in chemically single phase, which are characterized using dc magnetization, ac magnetic susceptibility, heat capacity, and neutron diffraction studies. Neutron diffraction and heat capacity studies confirm that long-range magnetic ordering coexists with the frustrated glassy magnetic components for both compounds. The static and dynamical features of dc magnetization and frequency-dependent ac susceptibility data reveal that Gd$_2$NiSi$_3$ is a canonical spin-glass system, while Er$_2$NiSi$_3$ is a reentrant spin cluster-glass system. The spin freezing temperature merges with the long-range antiferromagnetic ordering temperature at 16.4 K for Gd$_2$NiSi$_3$. Er$_2$NiSi$_3$ undergoes antiferromagnetic ordering at 5.4 K, which is slightly above the spin freezing temperature at 3 K. The detailed studies of nonequilibrium dynamical behavior, viz., the memory effect and relaxation behavior using different protocols, suggest that both compounds favor the hierarchical model over the droplet model. A large magnetocaloric effect is observed for both compounds. Maximum values of isothermal entropy change ($-\Delta S_M$) and relative cooling power (RCP) are found to be 18.4 J/kg K and 525 J/kg for Gd$_2$NiSi$_3$ and 22.6 J/kg K and 540 J/kg for Er$_2$NiSi$_3$, respectively, for a change in field from 0 to 70 kOe. The values of RCP are comparable to those of the promising refrigerant materials. A correlation between large RCP and magnetic frustration is discussed for developing new magnetic refrigerant materials.

I. INTRODUCTION

In the past decade, the magnetocaloric effect (MCE) -based magnetic refrigeration technique has attracted considerable attention due to its improved efficiency and its environmentally friendly nature [1–3]. The MCE is defined as a change in the temperature of materials due to the application of a magnetic field in an adiabatic condition. Typically, a large MCE involves a significant change in magnetic entropy, adiabatic temperature, and cooling power, and generally it is observed in the vicinity of a magnetic phase transition from paramagnetism to ferromagnetism [4–6]. It can also be observed in magnetic-field-induced metamagnetic transitions for antiferromagnetic compounds [7,8]. Recently, a new type of materials for the emerging large MCE have been theoretically proposed based on magnetic frustrations [9–11]. To the best of our knowledge, this theoretical prediction has been verified only on rare occasions [12,13].

In this work, we attempt to search for new magnetically frustrated systems that also exhibit a large MCE. We have identified ternary intermetallics of R_2TX_3-type (where R denotes rare earth, T denotes transition metal, and $X =$ Si,Ge,In, etc.) as promising candidates to achieve this goal. The R_2TX_3 compounds usually crystallize in a hexagonal AlB$_2$-type crystal structure with a $P6/mmm$ space group [14]. The R ions occupy Al positions and form a hexagonal structure of edge-sharing triangles, as depicted in Fig. 1(a). The other two ions (T and X) are randomly distributed between rare-earth ions containing two hexagonal layers, as shown in Fig. 1(b). Thus, the structure consists of alternative hexagonal layers of R ions and randomly distributed T-X ions along the hexagonal c axis. In these compounds, transition-metal ions are generally nonmagnetic, and exchange interaction between

rare-earth ions is of Ruderman-Kittel-Kasuya-Yosida (RKKY) type. Generally, antiferromagnetic interaction in the hexagonal plane favors magnetic frustration [15]. Magnetic frustration may also arise when nearest-neighbor exchange interaction strength J_1 and next-nearest-neighbor exchange interaction strength J_2 are of comparable and opposite sign [16]. In R_2TX_3-type compounds, lattice parameters a and c are close enough ($c/a \sim 1$), and a strong frustration may occur when J_1 and J_2 have opposite signs [17]. In addition, T and X ions are randomly distributed between two hexagonal layers of R ions, which causes a random variation in the RKKY-mediated exchange interaction. The coexistence of disorder and frustration are fundamental to perceiving the spin-glass state [18], which may also occur in R_2TX_3 series [19,20]. A significant volume of work has been done on R_2TX_3 series, with T as Pd, Cu, Pt, and Rh, and X as Si, Ge, and In [19,21–23]. However, investigations on R_2NiSi$_3$ series are ignored, except for Ce$_2$NiSi$_3$ [24].

An attempt to prepare chemically single-phase compounds of R_2NiSi$_3$ series was successful for Gd$_2$NiSi$_3$ and Er$_2$NiSi$_3$. We found an additional impurity phase in other members of the R_2NiSi$_3$ series. Our detailed ac susceptibility and dc magnetization studies confirm spin-glass and reentrant spin-glass frozen states at low temperature for Gd$_2$NiSi$_3$ and Er$_2$NiSi$_3$, respectively. Neutron diffraction on Er$_2$NiSi$_3$ and heat-capacity studies propose the possible magnetic ground states for both compounds. The considerable values of magnetic entropy change ($-\Delta S_M$) $\sim$18.4 and $\sim$22.6 J/kg K associated with the huge cooling power of $\sim$525 and $\sim$540 J/kg are revealed for Gd$_2$NiSi$_3$ and Er$_2$NiSi$_3$, respectively. A possible correlation between magnetic frustration and the observed large cooling power is discussed.
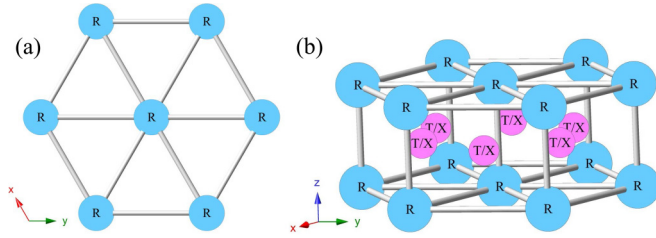
FIG. 1. R_2TX_3 crystal structure (AlB$_2$ type).

II. EXPERIMENTAL DETAILS

Polycrystalline samples were synthesized in an arc furnace by melting the appropriate amount of constituent elements of high purity (>99.9%) under an inert (Ar) atmosphere using a water-cooled Cu hearth. The ingots were remelted several times by flipping every time to promote volume homogeneity. The weight loss was less than 0.5%. Room-temperature and low-temperature (up to 15 K) x-ray diffraction (XRD) experiments were performed on the powdered as-cast samples using Cu $K\alpha$ radiation on a TTRAX-III diffractometer (M/s Rigaku, Japan) having 18 kW power. The crystal structure and phase purity were checked by Rietveld analysis of XRD data using the FULLPROF software package [25]. The dc magnetic measurements were carried out in SQUID VSM (M/s Quantum Design Inc., USA) and Ever Cool II VSM (M/s Quantum Design Inc., USA) in the temperature range 2–300 K and magnetic fields up to 70 kOe. The ac magnetic measurements were carried out in a commercial SQUID magnetometer (MPMS XL Ever Cool model, M/s Quantum Design Inc., USA). The zero-field heat-capacity measurements were carried out in a PPMS system (M/s Quantum Design Inc., USA) in the temperature range 2–300 K. Zero-field neutron diffraction experiments for Er$_2$NiSi$_3$ were performed at ECHIDNA beamline in ANSTO, Australia, at various temperatures.

III. RESULTS AND DISCUSSION

A. X-ray diffraction

The room-temperature powder XRD patterns for polycrystalline Gd$_2$NiSi$_3$ [Fig. 2(a)] and Er$_2$NiSi$_3$ [Fig. 2(d)] were analyzed by Rietveld structural refinement using FULLPROF software. The Rietveld refinements of the XRD data reveal that both compounds form in a single phase with space group $P6/mmm$ (No. 191). The details of crystallographic parameters obtained from the refinement are listed in Table I.

These two compounds do not show any structural transition down to 15 K, which is the lowest temperature achievable in our diffractometer [Figs. 2(b) and 2(c)]. The temperature dependence of the unit-cell volume of Gd$_2$NiSi$_3$ [inset: Fig. 2(b)] and Er$_2$NiSi$_3$ [inset: Fig. 2(c)] is plotted and fitted using the equation

$$V(T) = \gamma U(T)/K_0 + V_0, \qquad (1)$$

where V_0 is the cell volume at $T = 0$, K_0 is the bulk modulus, and γ is the Grüneisen parameter. $U(T)$ is the internal energy, which can be expressed according to the Debye approximation
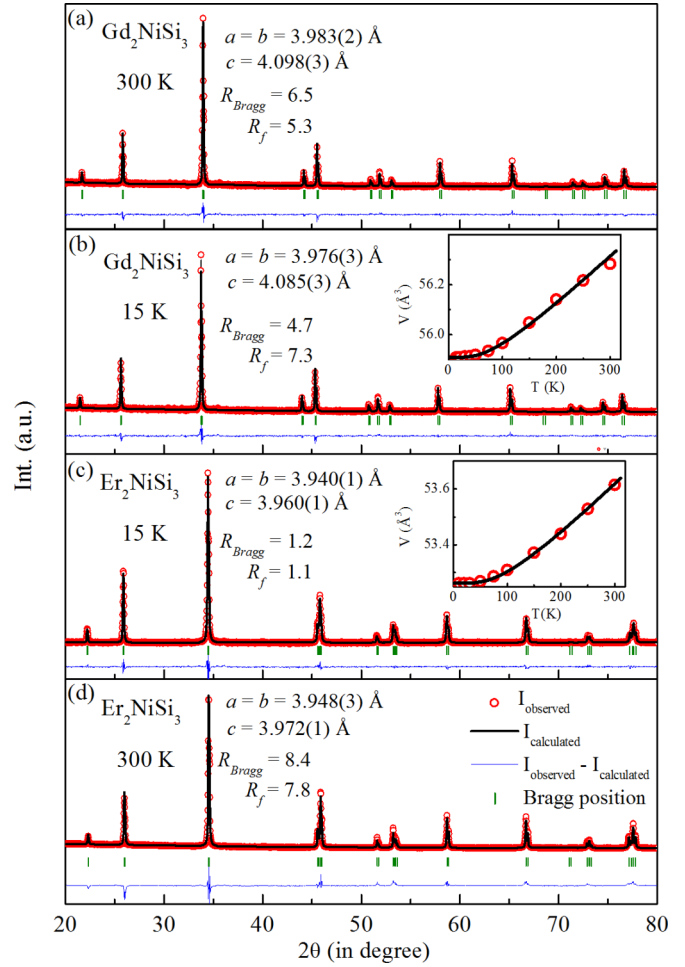

FIG. 2. (a) Room-temperature and (b) low-temperature ($T = 15$ K) XRD patterns along with Full-Rietveld refinement, of Gd$_2$NiSi$_3$. Inset (b): Temperature dependence of the unit-cell volume of Gd$_2$NiSi$_3$ along with a fit to Eq. (1). Full-Rietveld refinement of (c) room-temperature and (d) low-temperature ($T = 15$ K) XRD patterns of Er$_2$NiSi$_3$. Inset (c): Temperature dependence of the unit-cell volume of Er$_2$NiSi$_3$ along with a fit to Eq. (1).

TABLE I. Crystallographic and refinement parameters obtained from the structural analysis of room-temperature powder x-ray-diffraction data of Gd$_2$NiSi$_3$ and Er$_2$NiSi$_3$.

Compound	Gd$_2$NiSi$_3$		Er$_2$NiSi$_3$		
Structure	AlB$_2$-type hexagonal				
Space group	$P6/mmm$, No. 191				
Lattice parameters					
a (Å)	3.983(2)		3.948(3)		
c (Å)	4.098(3)		3.972(1)		
Cell volume, V_{cell} (Å^3)	56.315(1)		53.635(1)		
Atomic coordinates					
Atom	Wyckoff symbol	x	y	z	Occupancy
Gd	1a	0	0	0	0.0416(2)
Ni	2d	1/3	2/3	1/2	0.0212(3)
Si	2d	1/3	2/3	1/2	0.0622(3)
Er	1a	0	0	0	0.0416(2)
Ni	2d	1/3	2/3	1/2	0.0209(3)
Si	2d	1/3	2/3	1/2	0.0625(3)

as

$$U(T) = 9Nk_B T \left(\frac{T}{\Theta_D}\right)^3 \int_0^{\frac{\Theta_D}{T}} \frac{x^3}{e^x - 1} dx, \qquad (2)$$

where N is the number of atoms per unit cell. Using this approximation, Debye temperatures for the compound Gd_2NiSi_3 ($\Theta_D = 305 \pm 5$ K) and Er_2NiSi_3 ($\Theta_D = 360 \pm 5$ K) have been estimated. The lattice parameters a and c vary in same manner as the unit-cell variation with temperature.

B. dc magnetization

The dc magnetic susceptibility ($\chi = M/H$) of Gd_2NiSi_3 and Er_2NiSi_3, under both a zero-field-cooled (ZFC) and a field-cooled (FC) protocol as a function of temperature, are shown in Figs. 3(a) and 3(b), respectively, for different external applied magnetic fields. For Gd_2NiSi_3, both ZFC and FC susceptibility (M/H) show a peak around a temperature 16.4 K, denoted as T_N. The peak is broad in nature. The ZFC and FC curves start to diverge below a certain temperature, called the irreversible temperature, denoted as T_{irr} (=17 K). The difference between ZFC and FC magnetization becomes negligible above an applied field of 20 kOe. In the case of Er_2NiSi_3, magnetization shows an antiferromagnetic-type transition around a peak temperature 5.4 K, denoted as T_N. Around 3 K, an additional anomaly [clearly visible in the temperature derivative of ZFC magnetization; see the inset of Fig. 3(b)] can only be seen in ZFC magnetization under a low applied magnetic field. The temperature is referred to as the characteristic temperature and is denoted as T_f. The ZFC and FC curves diverge below the irreversibility temperature (T_{irr}) 5.4 K. In the paramagnetic region ($T > 60$ K for Gd_2NiSi_3, $T > 50$ K for Er_2NiSi_3), magnetic susceptibility follows the Curie-Weiss (CW) behavior $\chi(T) = \frac{C}{T - \theta_{CW}}$, where C is the Curie constant and θ_{CW} is the paramagnetic Curie-Weiss temperature. A linear fit to the inverse susceptibility curves yields $\theta_{CW} = 14.3$ and 0.8 K for Gd_2NiSi_3 [right inset, Fig. 3(a)] and Er_2NiSi_3 [right inset, Fig. 3(b)], respectively. The positive value of θ_{CW} signifies the presence of a ferromagnetic exchange interaction in the systems. The calculated values of the effective moments are 7.94 μ_B/Gd^{3+} ion and 9.80 μ_B/Er^{3+} ion, which are close to their respective theoretical free moment value [$g\sqrt{J(J+1)}$], indicating that only the localized $4f$ shells are contributing toward the magnetic properties.

For Gd_2NiSi_3 and Er_2NiSi_3, the peak temperature (T_N) and the characteristic temperature (T_f), respectively, shift to the lower-temperature region with an increase in applied magnetic field. The peak temperature ($T_N = 5.4$ K) is almost insensitive to the applied magnetic-field strength for Er_2NiSi_3. The peak temperatures [$T_P = T_N = T_f$ for Gd_2NiSi_3 (discussed in Sec. III C) and T_f for Er_2NiSi_3] and irreversible temperatures (T_{irr}) depend strongly on the applied magnetic-field strength for both compounds. Such a shift of peak temperature (T_P) and irreversible temperature (T_{irr}) under the application of an external magnetic field is typically observed for spin-glass systems [26]. In the low-field region, the variation of $T_P(H)$ and $T_{irr}(H)$ can be represented by the following equation:

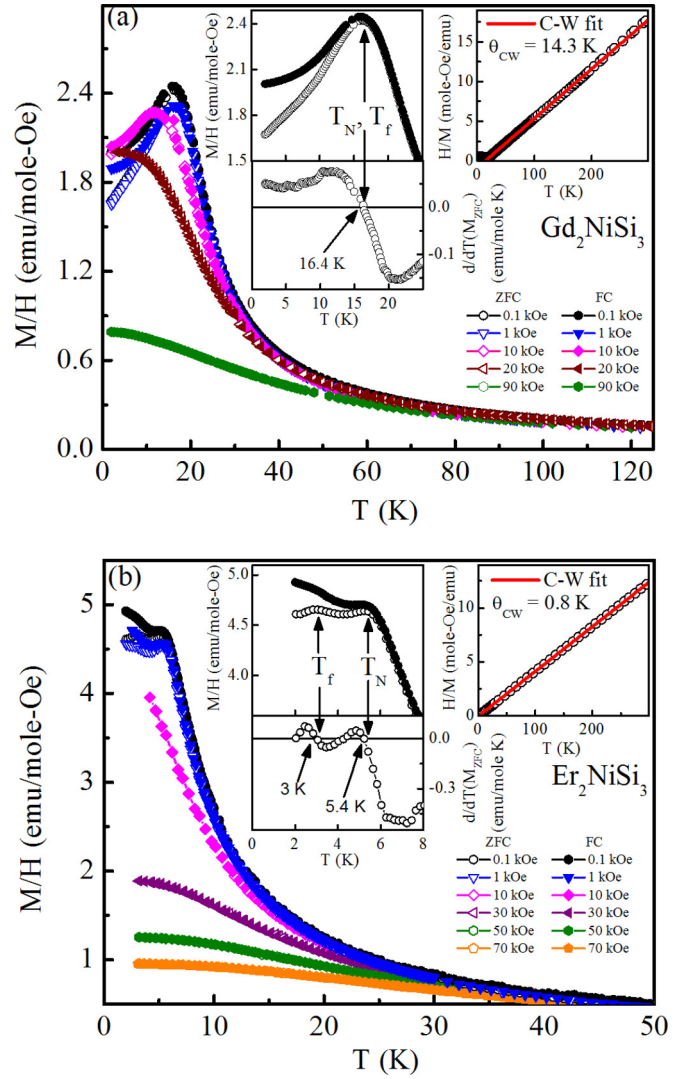$$T_{P,irr}(H) = T_{P,irr}(0)(1 - AH^n), \qquad (3)$$

FIG. 3. (a) Temperature dependence of dc magnetic susceptibility (M/H) for different magnetic fields of Gd_2NiSi_3 in zero-field-cooled (ZFC) and field-cooled (FC) mode. Left inset: expanded region of magnetic susceptibility around the transition temperature along with the temperature derivative of ZFC magnetization. Right inset: inverse susceptibility (H/M) as a function of temperature for $H = 100$ Oe. (b) M/H vs T of Er_2NiSi_3 for different magnetic fields in zero-field-cooled (ZFC) and field-cooled (FC) mode. Left inset: expanded region of M/H vs T around transition temperatures T_N and T_f along with the temperature derivative of ZFC magnetization. Right inset: H/M vs T for $H = 100$ Oe.

where A is a constant, and $T_{P,irr}(0)$ is T_P and T_{irr} in the absence of a magnetic field. The experimentally observed field dependence of T_P and T_{irr} along with the fit to the above equation are shown in Figs. 4(a)–4(d) for the compounds Gd_2NiSi_3 and Er_2NiSi_3, respectively. The values of $T_P(0)$ obtained from the fits are 16.4 and 3.1 K along with n values 2.04 (± 0.03) and 1.98 (± 0.04) for Gd_2NiSi_3 and Er_2NiSi_3, respectively. On the other hand, the obtained values of $T_{irr}(0)$ are 18 and 6 K along with n values 0.62 (± 0.03) and 0.6 (± 0.02) for Gd_2NiSi_3 and Er_2NiSi_3, respectively. Theoretically for spin-glass systems, in the H-T phase diagram, the spin freezing temperature with weak irreversibility follows the Gabay-Toulouse
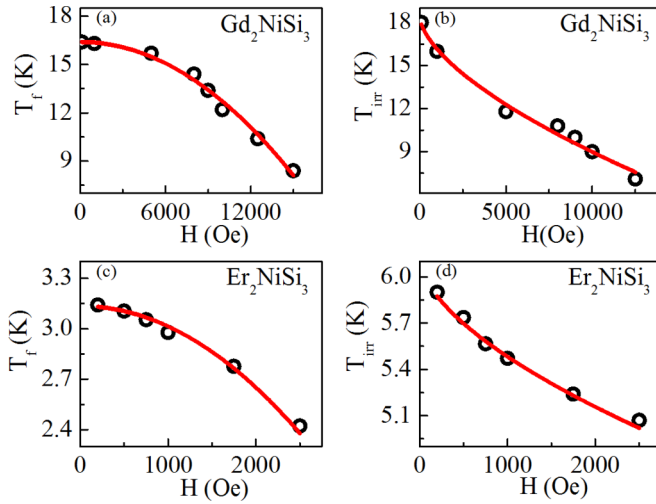
FIG. 4. Dependence of peak temperature (T_f) for (a) Gd_2NiSi_3 and (c) Er_2NiSi_3 and of irreversibility temperature (T_{irr}) for (b) Gd_2NiSi_3 and (d) Er_2NiSi_3 as a function of magnetic field. Solid lines are the fit to Eq. (3). For Gd_2NiSi_3, $T_N = T_f$ (see Sec. III C).

(GT) line ($T_f \propto H^2$), while the Almeida-Thouless (AT) line ($T_f \propto H^{2/3}$) is obeyed by the system with strong irreversibility characteristics [27,28]. The experimentally obtained field exponents of $T_P(H)$ and $T_{irr}(H)$ from dc magnetization results for both Gd_2NiSi_3 and Er_2NiSi_3 are found to be quite similar to those of the two lines. Similar behavior had been reported earlier for quite a few other systems [29–31]. It may be noted that the dc magnetization results only provide some hints of the formation of metastable states below these characteristic temperatures. Exact experimental determination of GT and AT lines needs to be performed through the precise determination of the freezing temperature over a wide magnetic-field range along with verification of critical slowing down behavior [18].

C. ac susceptibility

To understand the underlying nature of magnetic transitions determined from dc magnetization, ac susceptibility measurements were carried out in an excitation field of 4 Oe for various frequencies (f). In Figs. 5(a) and 5(b), the real part of the ac susceptibility (χ') as a function of temperature for various frequencies is plotted for Gd_2NiSi_3 and Er_2NiSi_3, respectively. In the case of Er_2NiSi_3, the peak temperature (T_N) 5.4 K is frequency-independent, whereas the characteristic peak temperature (T_f) around 3 K shifts toward higher temperatures with increasing frequencies (3 K for $f = 1.1$ Hz and 3.25 K for $f = 999.9$ Hz). The transition around 5.4 K reflects the long-range antiferromagnetic spin arrangement, whereas the transition around 3 K corresponds to the spin-glass freezing. Thus the compound Er_2NiSi_3 is a reentrant spin-glass material with a spin freezing temperature $T_f = 3$ K. On the other hand, as seen from Fig. 5(a), for Gd_2NiSi_3 the peak temperature (T_N) shifts to higher temperature with an increase in frequency (16.4 K for $f = 1.1$ Hz and 16.6 K for $f = 999.9$ Hz). This shift in peak temperature with increasing frequencies signifies a spin-glass transition in Gd_2NiSi_3 with $T_f = 16.4$ K. In a typical glassy system, the relative shift in freezing temperature
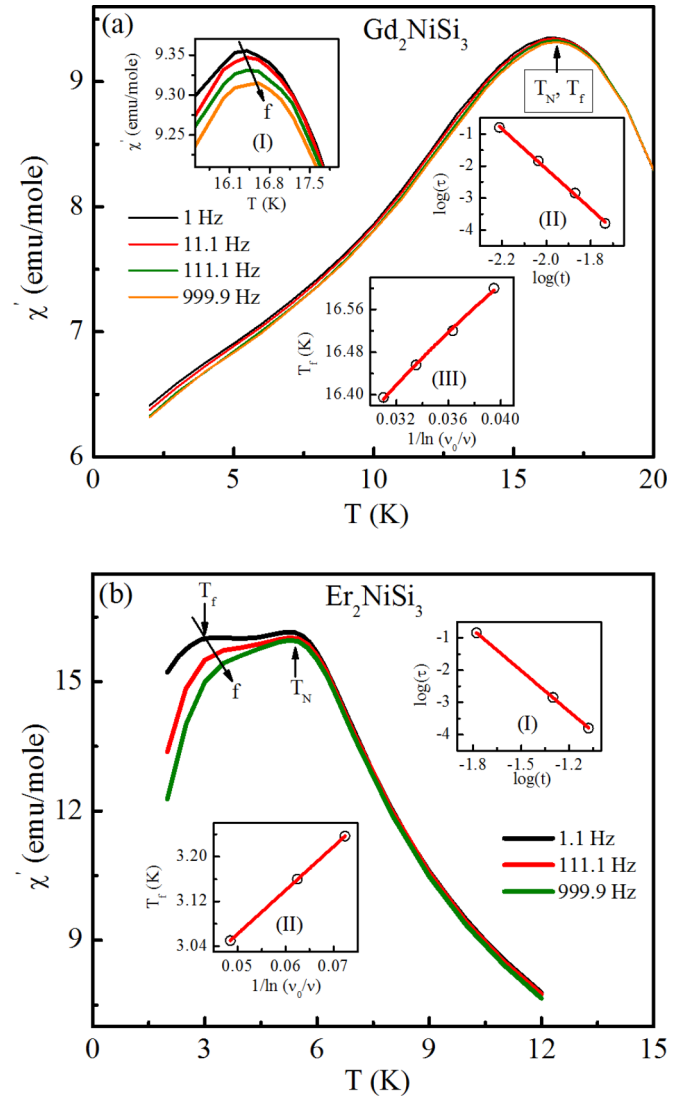

FIG. 5. The temperature dependence of the real part of the ac magnetic susceptibility of (a) Gd_2NiSi_3 and (b) Er_2NiSi_3 at different frequencies. An expanded region of Gd_2NiSi_3 around the freezing temperature is shown in inset I of part (a). The frequency dependence of the freezing temperature is shown in inset II of part (a) for Gd_2NiSi_3 and inset I of part (b) for Er_2NiSi_3, where $\ln(\tau)$ is plotted as a function of $\ln(t)$, with $t = (T_f - T_{SG}/T_{SG})$. The solid lines represent the fit to the power-law divergence. The frequency dependence of the freezing temperature is plotted as T_f vs $\ln(\nu_0/\nu)$ for Gd_2NiSi_3 [inset III of part (a)] and Er_2NiSi_3 [inset II of part (b)]. The solid line represents the fit to the Vogel-Fulcher law.

per decade of frequency is generally expressed as [18]

$$\delta T_f = \frac{\Delta T_f}{T_f \Delta(\log_{10}\nu)}. \qquad (4)$$

We found $\delta T_f = 0.004$ for Gd_2NiSi_3 and $\delta T_f = 0.02$ for Er_2NiSi_3. The calculated value of δT_f for Gd_2NiSi_3 lies typically in a range that is observed for canonical spin-glass systems. In the case of Er_2NiSi_3, the value is one order of magnitude higher than that for canonical spin-glass systems, and one order lower than that observed in typical superparamagnetic systems. The value is in the range generally observed

in spin cluster-glass compounds [18]. In spin-glass systems, the frequency dependence of T_f follows the conventional power-law divergence of a critical slowing down [18,32],

$$\tau = \tau_0 \left(\frac{T_f - T_{SG}}{T_{SG}} \right)^{-z\nu'}, \qquad (5)$$

where τ is the relaxation time associated with the measured frequency ($\tau = 1/\nu$), τ_0 is the single spin-flip relaxation time, T_{SG} is the spin-glass temperature (for $f = 0$), and $z\nu'$ is the dynamic critical exponent [ν' is the critical exponent of correlation length, $\xi = (T_f/T_{SG} - 1)^{-\nu'}$, and $\tau \sim \xi^z$]. Typically, $z\nu'$ lie between 4 and 12 for a spin-glass system. From our experimental results, we have found that $\tau_0 \simeq 10^{-13}$ s and $z\nu' = 6$ for Gd_2NiSi_3 [inset II, Fig. 5(a)] and $\tau_0 \simeq 10^{-9}$ s and $z\nu' = 4$ for Er_2NiSi_3 [inset I, Fig. 5(b)]. The value of τ_0 for Gd_2NiSi_3 is in the characteristic range of canonical spin-glass ($\sim 10^{-12} - 10^{-13}$) [30]. For Er_2NiSi_3, τ_0 is a few orders higher than that of typical canonical spin-glass, but in the range of typical spin cluster-glass systems [33].

Another dynamical scaling law in spin-glass freezing is the Vogel-Fulcher relation [18,34], where the frequency dependence of freezing temperature T_f is described by

$$\nu = \nu_0 \exp\left(-\frac{E_a}{K_B(T_f - T_0)} \right), \qquad (6)$$

where ν_0 denotes the characteristic attempt frequency, E_a is the activation energy, and T_0 is the Vogel-Fulcher temperature. The best estimated values are $\frac{E_a}{K_B} = 23.83$ K and $T_0 = 15.65$ K for Gd_2NiSi_3 [inset III, Fig. 5(a)] and $\frac{E_a}{K_B} = 8.33$ K and $T_0 = 2.7$ K for Er_2NiSi_3 [inset II, Fig. 5(b)]. For canonical spin-glass systems, $\frac{E_a}{K_B}/T_0$ is generally found to be close to 1, while for spin cluster-glass systems the ratio is generally found to be relatively larger. Thus, the values of ~ 1.5 and 3.1 found for Gd_2NiSi_3 and Er_2NiSi_3, respectively, suggest that the former is a canonical spin-glass, while the latter is of a spin cluster-glass type.

D. Nonequilibrium dynamics

1. Wait-time-dependent magnetic relaxations and aging effect

Different kinds of frustrated glassy systems are characterized by their magnetic relaxation behavior. The relaxation process is measured in both ZFC and FC conditions. In the ZFC condition, the sample is cooled under zero applied magnetic field from the paramagnetic region to a desired temperature, which is below freezing. After waiting for a certain time at that temperature, a small amount of magnetic field is applied, and the time evolution of magnetization [$M(t)$] is measured. In the FC condition, the sample is cooled in the presence of a small magnetic field, from the paramagnetic region to the desired temperature (below freezing). After waiting for a certain time at the required temperature, the magnetic field is switched off and the time dependence of magnetization [$M(t)$] is measured. Figures 6(a) and 6(b) show the relaxation of ZFC magnetization for Gd_2NiSi_3 and Er_2NiSi_3, respectively, at 2 K, for different wait times at the particular temperature (2 K) before the relaxation processes start. For each relaxation process, the sample was cooled in zero field from the paramagnetic region ($T > 60$ K for Gd_2NiSi_3 and $T > 50$ K for Er_2NiSi_3) to the
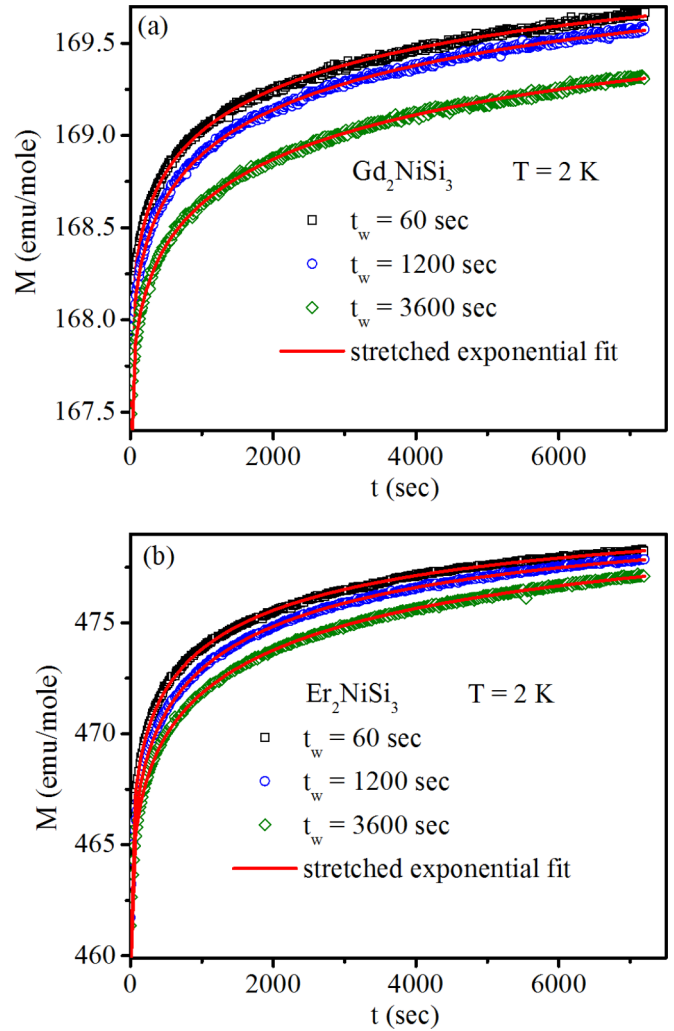

FIG. 6. Relaxation of zero-field-cooled (ZFC) magnetization for different wait times at $T = 2$ K for (a) Gd_2NiSi_3 and (b) Er_2NiSi_3. Solid red lines depict the fit of the relaxation data to the equation $M(t) = M_0 - M_g \exp[-(\frac{t}{\tau})^\beta]$.

measured temperature 2 K (lowest achievable temperature in our measurement system). After a lapse of wait time $t_w = 60$, 1200, and 3600 s, the time evolution of the magnetization [$M(t)$] was recorded after switching on the magnetic field of 100 Oe. The time dependence of the magnetization follows the standard stretched exponential function [31,35] of the form

$$M(t) = M_0 - M_g \exp\left[-\left(\frac{t}{\tau} \right)^\beta \right], \qquad (7)$$

where M_0 is an intrinsic magnetization, M_g is related to a glassy component of magnetization, τ is the characteristic relaxation time constant, and β is the stretching exponent. Typically, spin-glass systems are characterized by a distribution of energy barriers, and the value of β lies between 0 and 1 [18,36]. For both compounds, the value of β is found between 0.33 and 0.35, which are within the range of different glassy systems reported earlier [18,36]. The value of τ increases with wait time t_w, indicating the stiffening of the spin relaxation or the aging effect. In a spin-glass system, during the aging process, the wait-time-dependent magnetic relaxation process
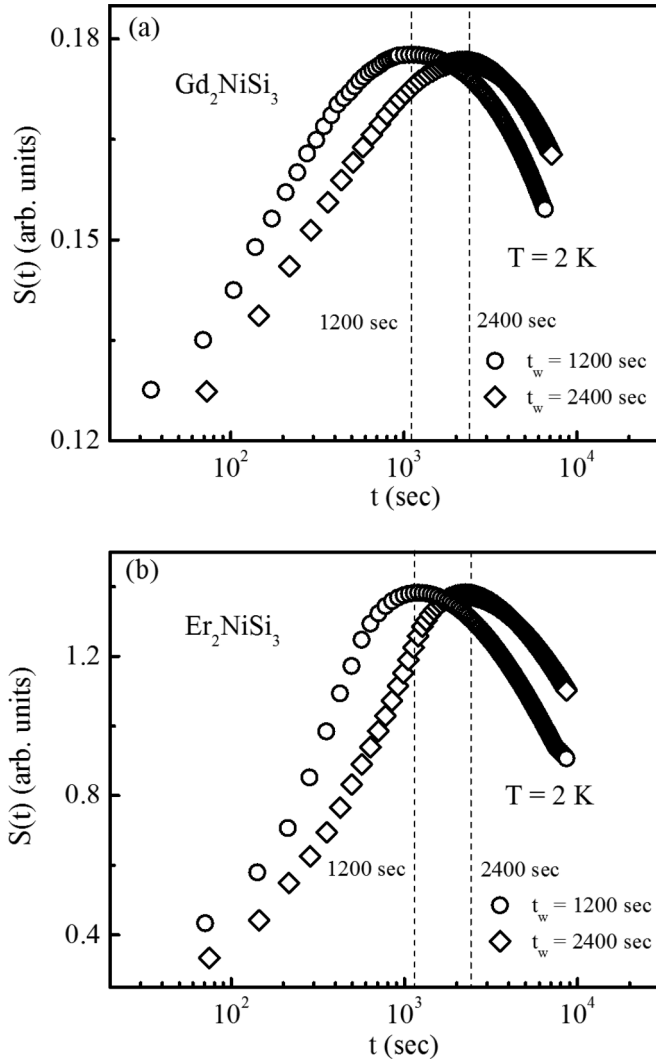
FIG. 7. The relaxation rate $S(t)$ (discussed in the text) at $T = 2$ K, in a field of 100 Oe after waiting for $t_w = 1200$ and 2400 s in zero field of (a) Gd$_2$NiSi$_3$ and (b) Er$_2$NiSi$_3$.

implies that the system is in a nonequilibrium state during the wait time and remembers the waiting time before the application of a magnetic field. The time dependence of the magnetization shows an inflection point at t_w. This inflection point can be clearly detected by the presence of a peak at $t \approx t_w$ in the magnetic viscosity, $S(t) = (1/H)\frac{dM(t)}{d(\log t)}$ plot as a function of time (t). The magnetic viscosity is obtained from the logarithmic time derivative of ZFC magnetization [18,37,38]. The inflection point corresponds to a maximum in the $S(t)$ curve, and it shifts to a longer observation time with an increase in t_w. Figures 7(a) and 7(b) show the aging curve at $T = 2$ K for Gd$_2$NiSi$_3$ and Er$_2$NiSi$_3$, respectively, for wait time $t_w = 1200$ and 2400 s. $S(t)$ curves attain a maximum close to the wait time t_w. This type of aging phenomenon describes the nonequilibrium dynamics of domain growth in spin-glass systems.

2. Magnetic memory effect

The memory effect in FC and ZFC protocols has been investigated following the protocol of Sun *et al.* [39] for

both compounds. In the FC process, the samples were cooled with 100 Oe applied magnetic field from the paramagnetic region ($T > 60$ K for Gd$_2$NiSi$_3$ and $T > 50$ K for Er$_2$NiSi$_3$) to the lowest temperature (2 K) with intermediate stops at $T_{\mathrm{stop}} = 3$, 6, and 9 K for Gd$_2$NiSi$_3$ [Fig. 8(a)] and 2.5 and 4.5 K for Er$_2$NiSi$_3$ [Fig. 8(b)] of duration $t_w = 1.5$ h, and the magnetization [$M(T)$] was recorded. At the stopping temperatures, the magnetic field was turned off, and after the lapse of t_w the same field was reapplied with resumed cooling. This observed magnetization in this process is depicted as $M_{\mathrm{fcc}}^{\mathrm{stop}}$. After reaching 2 K, the samples were heated back to the paramagnetic region with the same applied field, and the magnetization [$M(T)$] was recorded. $M_{\mathrm{FCW}}^{\mathrm{mem}}$ curves thus obtained exhibit a clear signature of the past history of the magnetization, as it attempts to follow $M_{\mathrm{FCC}}^{\mathrm{stop}}$ curves. The conventional FC magnetization curves ($M_{\mathrm{FCW}}^{\mathrm{ref}}$) are also shown in Figs. 8(a) and 8(b) for the compounds. In the case of both compounds, a magnetic memory effect is observed below their respective freezing temperatures. Since for Er$_2$NiSi$_3$ $T_f < T_N$, no memory effect is observed in the dominating magnetically ordered region above T_f ($T_f < T < T_N$). The FC memory effects obtained for both compounds are quite similar to those observed in various spin-glass systems [35,40].

The memory effect can also be seen in phase-separated or superparamagnetic systems in the FC protocol, but not in the ZFC protocol [41]. Only the spin-glass systems are known to exhibit the memory effect in the ZFC protocol. In measuring the ZFC memory effect, the sample was first cooled in zero field from the paramagnetic region to some stopping temperatures ($T_{\mathrm{stop}} = 3$, 6, and 9 K for Gd$_2$NiSi$_3$ [Fig. 8(c)] and 3 and 4.5 K for Er$_2$NiSi$_3$ [Fig. 8(d)]), where the temperature was maintained for 1 h. The cooling was then resumed down to the lowest temperature. After applying a magnetic field (in our case 100 Oe), magnetization [$M(T)$] was recorded during heating. This magnetization curve is designated as $M_{\mathrm{ZFCW}}^{\mathrm{mem}}$. The conventional ZFC magnetization (for $H = 100$ Oe) was also recorded. This is depicted as $M_{\mathrm{ZFCW}}^{\mathrm{ref}}$. The ZFC memory effects are shown in Figs. 8(c) and 8(d) for Gd$_2$NiSi$_3$ and Er$_2$NiSi$_3$, respectively. For Gd$_2$NiSi$_3$ the difference curve ΔM ($= M_{\mathrm{ZFCW}}^{\mathrm{mem}} - M_{\mathrm{ZFCW}}^{\mathrm{ref}}$) exhibits memory dips at the stopping temperatures, which are below the freezing temperature. Expectedly, for Er$_2$NiSi$_3$ such memory dips can only be observed at 3 K (below freezing temperature), while no memory dip is observed around 4.5 K (above freezing temperature). These memory dips in the ZFC mode also confirm spin-glass behavior in these compounds and establish that this glassy behavior in the compounds is due to cooperative spin-spin interactions [41].

Such memory effects in glassy systems can be described by two theoretical models, viz., the droplet [42,43] and the hierarchical model [44,45]. At a particular temperature, only one spin configuration favors the droplet model, whereas a multivalley structure is formed on the free-energy landscape in the hierarchical model. Experimentally the two models can be distinguished by determining the presence or absence of the original spin configuration after a positive temperature cycle. The original spin configuration is restored in the droplet model, while temporary heating rejuvenates the original spin configuration in the hierarchical model. To understand the mechanism of the memory effect exhibited by these two
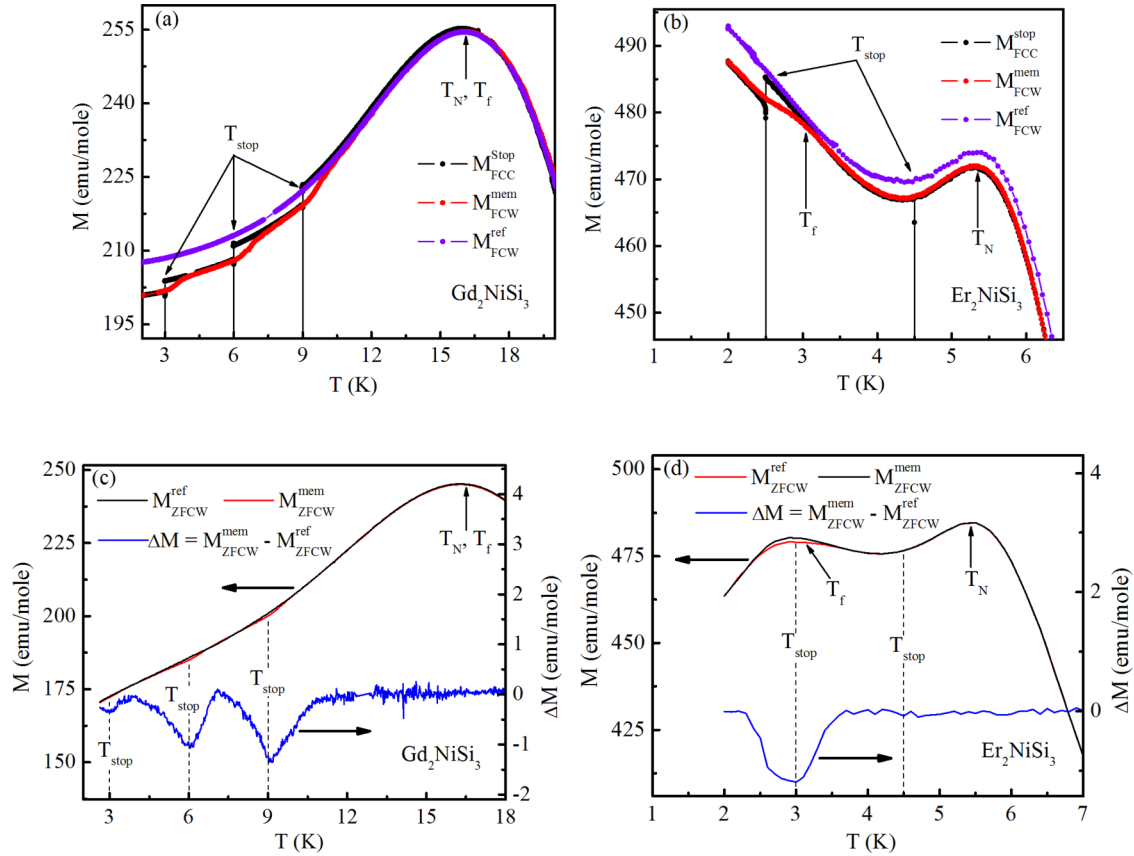
FIG. 8. Memory effect of Gd_2NiSi_3 in (a) FC and (c) ZFC protocol, as discussed in the text. Memory effect of Er_2NiSi_3 in (b) FC and (d) ZFC protocol. (Details are in the text.)

spin-glass systems, the influence of temperature cycling on magnetic relaxation behavior was investigated following the protocol of Sun *et al.* [39]. Magnetic relaxation behavior with temporary cooling under ZFC and FC conditions for the compounds Gd_2NiSi_3 and Er_2NiSi_3 is shown in Figs. 9(a),9(c) and Figs. 9(b),9(d), respectively. In the ZFC magnetic relaxation process, the sample was cooled down to a temperature T_0 (4 K for Gd_2NiSi_3 and 3 K for Er_2NiSi_3) in zero field ($T_0 < T_f$). Then a field of 100 Oe was applied and the magnetization was recorded for $t_1 = 1$ h. The sample was then quenched to a lower temperature $T_0 - \Delta T$ (2 K for both Gd_2NiSi_3 and Er_2NiSi_3) at a constant field, and the magnetization [$M(t)$] was recorded for $t_2 = 1$ h. Finally, the temperature was turned back to T_0 and the magnetization [$M(t)$] was recorded for another time period $t_3 = 1$ h. In the FC process, initially the sample was cooled to T_0 under an applied field 100 Oe and the same process as ZFC was performed after switching off the magnetic field. From Figs. 9(a)–9(d) it is clear that when the temperature is raised back to T_0, the magnetization comes back to the level it reached before temporary cooling in both ZFC and FC processes. The relaxation curve during t_3 is a continuation of that during t_1, and it can be fitted to a single curve following the stretched exponential form [$M(t) \sim \exp(-\frac{t}{\tau})^\beta$; $(0 < \beta < 1)$], with $\beta = 0.33$ for Gd_2NiSi_3 and 0.35 for Er_2NiSi_3, which are similar to that obtained from the relaxation process, often

observed in spin-glass systems [18]. This type of behavior suggests that the memory effect is quite strong for both of these two compounds below their respective freezing temperatures.

The effect of positive temperature cycling in both ZFC and FC mode has also been investigated, as shown in Figs. 9(e) and 9(f) for both compounds. In the ZFC process, the sample was cooled down to a temperature T_0 (4 K for Gd_2NiSi_3 and 2 K for Er_2NiSi_3) in zero field ($T_0 < T_f$). Then a field of 100 Oe was applied, and the magnetization [$M(t)$] was recorded for $t_1 = 1$ h. The sample was then heated to a higher temperature $T_0 + \Delta T$ (6 K for Gd_2NiSi_3 and 3 K for Er_2NiSi_3) at a constant field, and the magnetization was recorded for $t_2 = 1$ h. Finally, the temperature was again turned back to T_0 and the magnetization was recorded for another time period $t_3 = 1$ h. Due to the positive cycling of temperature, the magnetization at the beginning of t_3 does not come back to the level it had reached just before temporary heating, and the nature of magnetic relaxation during the time period t_3 is quite different from that during t_1. Similar behavior has also been observed for the FC method. Thus, positive temperature cycling rejuvenates the magnetic relaxation process, and hence no memory effect can be observed. Thus, the asymmetric response in the negative and positive temperature change favors the hierarchical model of the relaxation for both compounds. The above studies on magnetic relaxation and the memory effect confirm the spin-glass phase in these compounds.
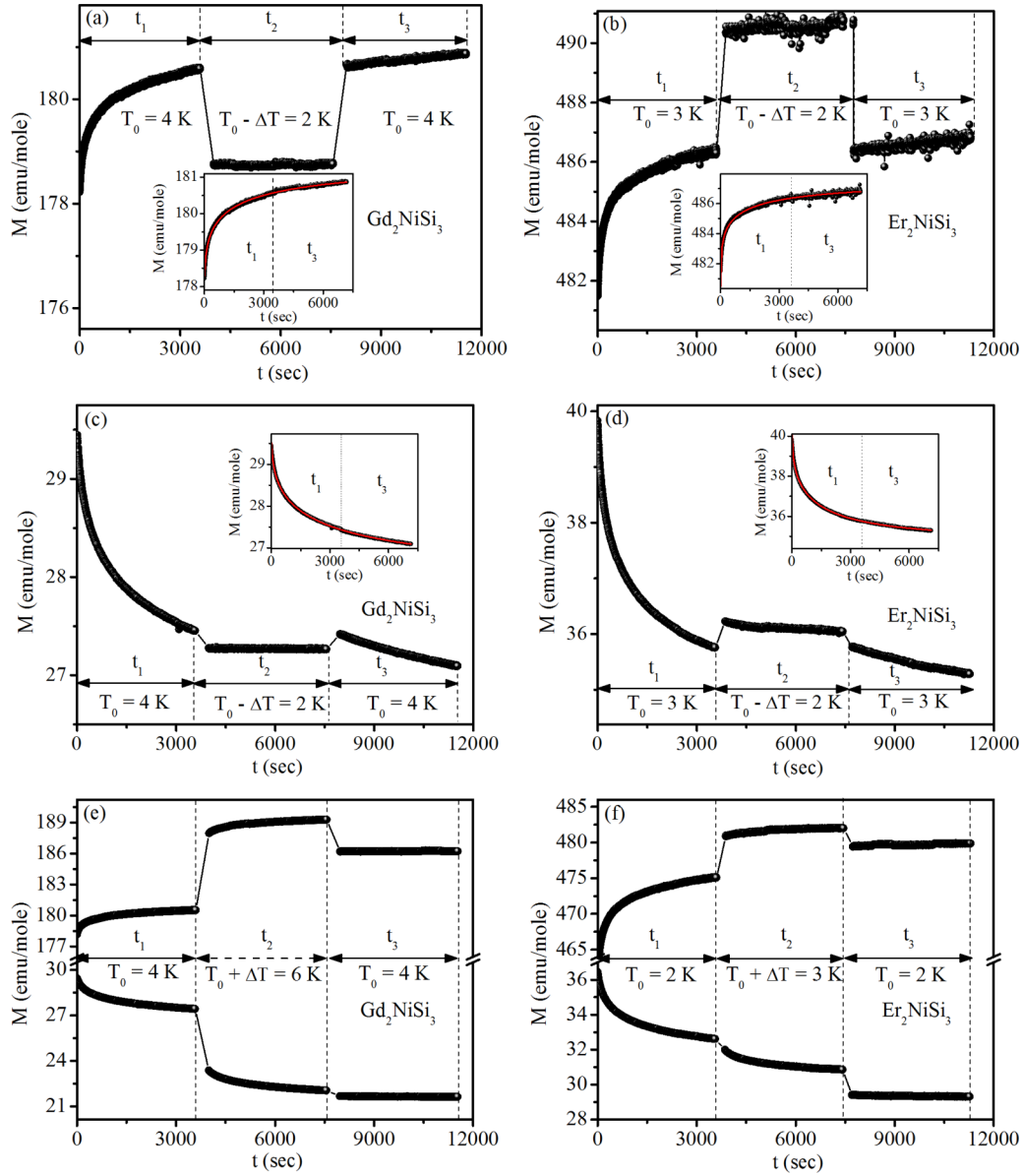
FIG. 9. Magnetic relaxation at 4 K for $H = 100$ Oe with temporary cooling at 2 K in the ZFC method (a) and the FC method (c) for Gd_2NiSi_3. Insets show the same data vs the total time spent at 4 K. Magnetic relaxation at 3 K for $H = 100$ Oe with temporary cooling at 2 K in the ZFC method (b) and the FC method (d) for Er_2NiSi_3. Insets show the same data vs the total time spent at 3 K. Magnetic relaxation at 4 K with temporary heating at 6 K in the ZFC method and the FC method for $H = 100$ Oe for Gd_2NiSi_3 (e). Magnetic relaxation at 2 K with temporary heating at 3 K in the ZFC method and the FC method for $H = 100$ Oe for Er_2NiSi_3 (f).

3. Temperature-dependent magnetic relaxations

Spin-glass behavior can originate from individual spin freezing, and it can also be due to the freezing of spin clusters. To determine whether the temperature dependence of magnetic relaxation is dependent on the presence of any interacting clusters in the systems, the magnetic relaxation behavior at different temperatures for the two compounds has been analyzed using a theoretical model by Ulrich *et al.* [46]. According to this model, the relaxation rate of the remanent magnetization $W(t) = -(d/dt)\ln M(t)$ for an assembly of interacting clusters decays according to the following law:

$$W(t) = At^{-n}, \quad t \geqslant t_0, \quad (8)$$

where A is a constant, n is an exponent function of temperature, and t_0 is the crossover time. The value of n is very important as it depends on the density of particles, and it is a measure of the strength of the dipolar interaction among the magnetic clusters taking part in the relaxation process. For a canonical spin-glass system, the values of n remain constant over the temperature region below freezing, whereas for spin cluster-glass systems, values of n vary in the temperature region around freezing. Figures 10(a) and 10(b) depict the relaxation rate W of the thermoremanent magnetization (TRM) as a function of temperature in a $\log_{10}$-$\log_{10}$ scale for different temperatures for both compounds. The thermoremanent magnetization was measured by cooling the sample in zero magnetic field to the desired temperature, below freezing. After waiting for
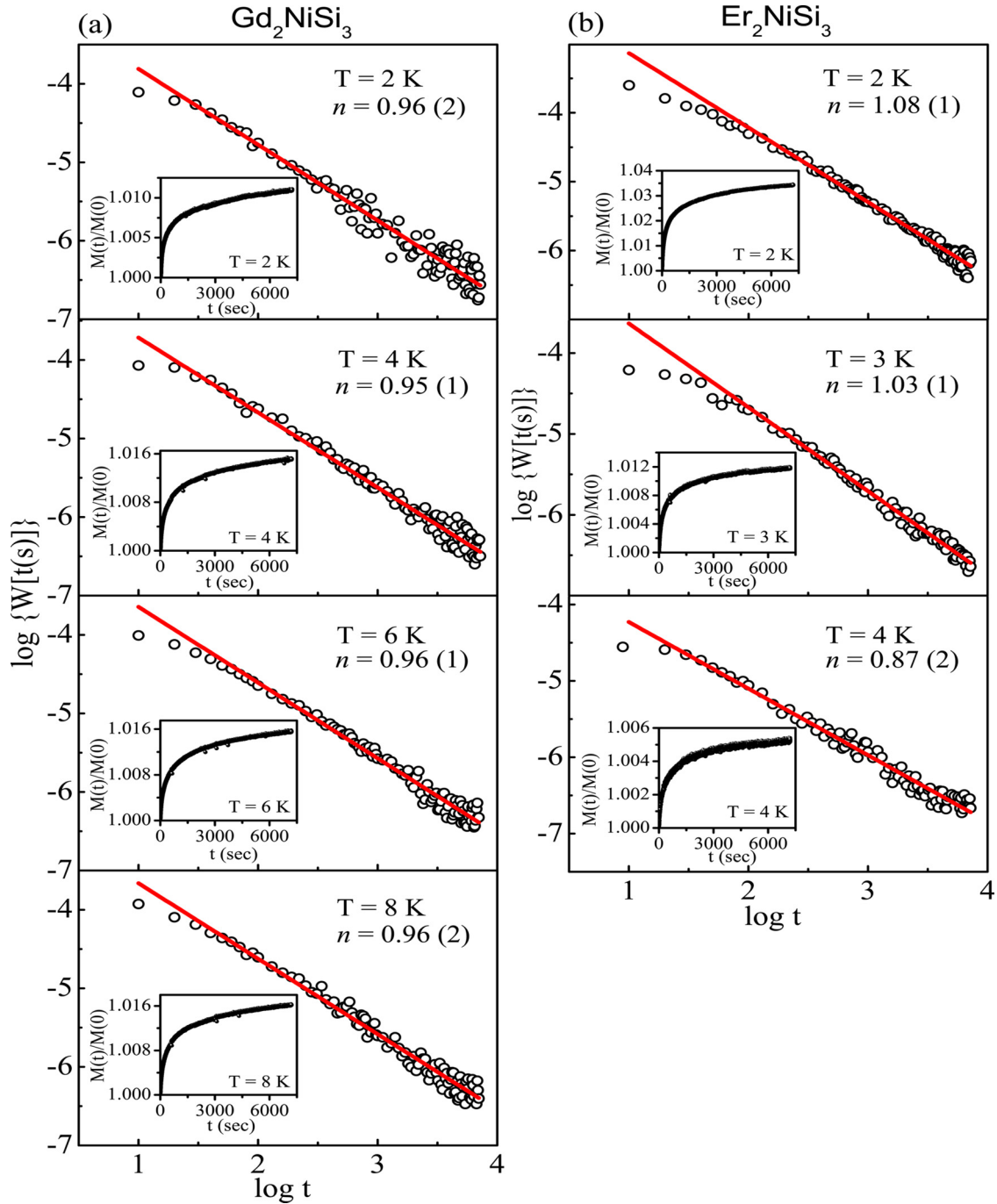
FIG. 10. (a) The magnetic relaxation rate as a function of time at 2, 4, 6, and 8 K on a $\log_{10}$-$\log_{10}$ plot for Gd_2NiSi_3. The solid red line is a linear fit to Eq. (8). (b) Time dependence of the magnetic relaxation rate at 2, 3, and 4 K on a $\log_{10}$-$\log_{10}$ scale for Er_2NiSi_3. The linear fit to Eq. (8) is depicted by a solid red line.

some time (in our case 60 s), a magnetic field was applied, and the time evolution of magnetization [$M(t)$] was recorded. The value of n remains insensitive to temperature for Gd_2NiSi_3, which is not the case for Er_2NiSi_3. For Er_2NiSi_3, n obtained from the relaxations at 2, 3, and 4 K is 1.08 (1), 1.03 (1), and 0.87 (2), respectively. This analysis according to the Ulrich condition strongly indicates that Gd_2NiSi_3 is a canonical spin-glass, whereas Er_2NiSi_3 is a reentrant spin cluster-glass.

E. Neutron diffraction

The neutron diffraction study of Er_2NiSi_3 under zero field is carried out at different temperatures in the range 1.5–10 K. The 10 K neutron diffraction pattern [lower panel, Fig. 11(a)] shows the nuclear Bragg peaks corresponding to the crystal structure. At 1.5 K [upper panel, Fig. 11(a)], new peaks of magnetic origin are observed pointing to antiferromagnetic reflections. Analysis of the neutron diffraction data indicates that the peaks of magnetic origin in the diffraction pattern can be
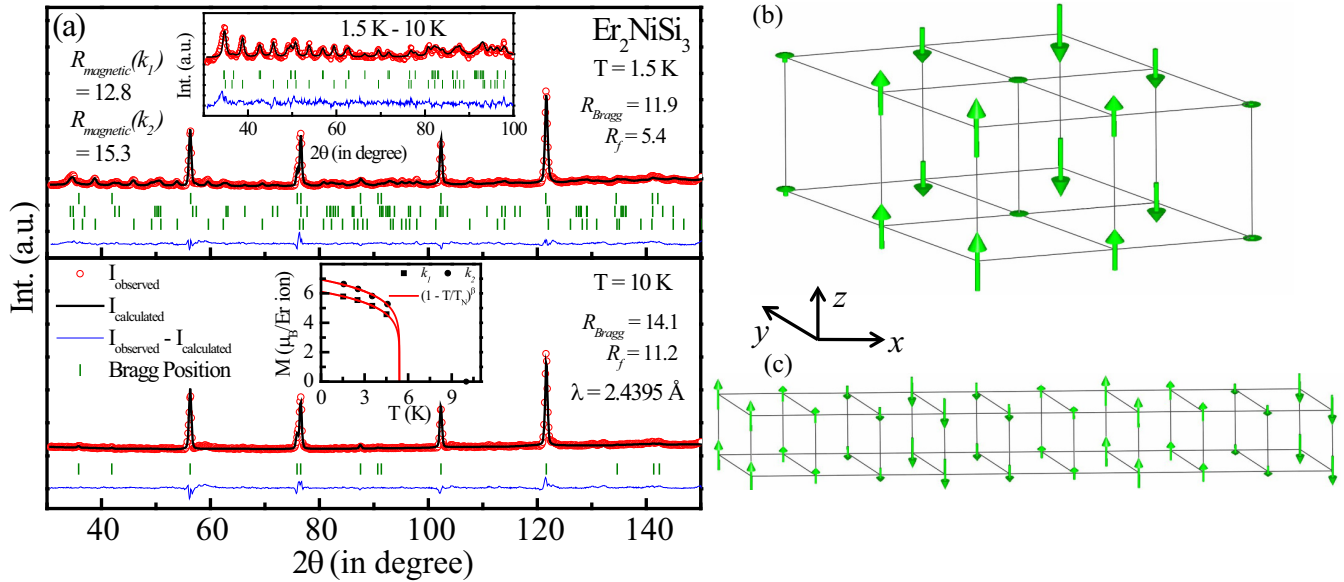
FIG. 11. Zero-field neutron diffraction pattern of Er_2NiSi_3 at $T = 10$ K [lower panel, part (a)] and $T = 1.5$ K [upper panel, part (a)] along with Rietveld refinement. The magnetic contribution of the diffraction pattern for $T = 1.5$ K is shown in the inset of the upper panel of part (a). Temperature dependence of the ordered magnetic moments for the two magnetic phases are shown in an inset in the lower panel of part (a). The magnetic structures corresponding to propagation vectors $k_1 = (0.1278, 0.1124, 0)$ and $k_2 = (0.1634, 0, 0)$ are shown in (b) and (c), respectively.

indexed with two propagation vectors $k_1 = (0.1278, 0.1124, 0)$ and $k_2 = (0.1634, 0, 0)$ with moment values $5.8\,\mu_B$ and $6.6\,\mu_B$, respectively. Two magnetic structures corresponding to the two propagation vectors are shown in Figs. 11(b) and 11(c). The magnetic peaks along with some other peaks are diffusive in nature. The broad diffuse peak becomes broader and weaker as the temperature is raised, corresponding to the thermal disruption of the magnetic correlations. Although the height of the short-range-order peak continues to increase down to $T = 1.5$ K, which is the lowest temperature in this study, it is expected to saturate out at sufficiently low temperature well below the freezing temperature. This diffuse nature of the scattered magnetic peaks corresponds to the presence of at least three magnetically different macroscopic phases, one corresponding to k_1, another to k_2, and another that occurs due to the short-range interaction of the magnetically frustrated moments. The presence of short-range correlations in the system is often seen in glassy materials with magnetic frustration, which usually exist in a low-dimensional energy scale [47–49]. Using the internal FULLPROF routines for microstructural analysis, the correlation length was estimated at 1.5 K to be $\sim$250 Å. The value gradually reduces to $\sim$143 Å at 4.5 K. Although short-range correlations persist above the ordering temperature, as evidenced by the deviation of the inverse susceptibility from linearity below 50 K, and there is likely a contribution of diffuse magnetic scattering to the background in the neutron diffraction data collected at 10 K, the high density of magnetic peaks did not allow us to resolve them and extract a correlation length value at that temperature.

F. Heat capacity

Figures 12(a) and 12(b) show zero-field heat capacity as a function of temperature for Gd_2NiSi_3 and Er_2NiSi_3,

respectively. For both compounds, a broad peak around T_N is observed, while no peak is observed around T_f for Er_2NiSi_3. The broad peak in the two compounds indicates the presence of long-range magnetic order along with the frustrated spin-glass phase, similar to that observed for early reported spin-glass compounds [20,21,50,51].

According to the mean-field theory [52], the jump in heat capacity at transition temperature can be predicted for an equal moment (EM) structure, where magnetic moments are the same on all sites, as

$$\Delta C_{EM} = 5 \frac{J(J+1)}{(2J^2 + 2J + 1)} R \qquad (9)$$

and for amplitude modulated (AM) structure, where the magnetic moment amplitude varies periodically from one site to another,

$$\Delta C_{AM} = \frac{10}{3} \frac{J(J+1)}{(2J^2 + 2J + 1)} R, \qquad (10)$$

where J is the total angular momentum and R is the universal gas constant (8.314 J mol^{-1} K^{-1}). The calculated theoretical values of ΔC_{EM} and ΔC_{AM} for a Gd^{3+} ion are 20.14 and 13.43 J/mol K, respectively. The calculated experimental value is $\Delta C \simeq 17$ J/mol Gd K for Gd_2NiSi_3. For the compound, ΔC is greater than the theoretical ΔC_{EM} value and less than the theoretical ΔC_{AM} value. This also implies that all the moments are not taking part in the ordering process simultaneously, and it favors macroscopically different magnetic phases in the compound Gd_2NiSi_3. According to this theoretical model, the jump in heat-capacity peak around the transition temperature cannot be estimated for Er_2NiSi_3 due to the presence of crystal electric fields, and because the model is developed without considering the presence of crystal-field effects.
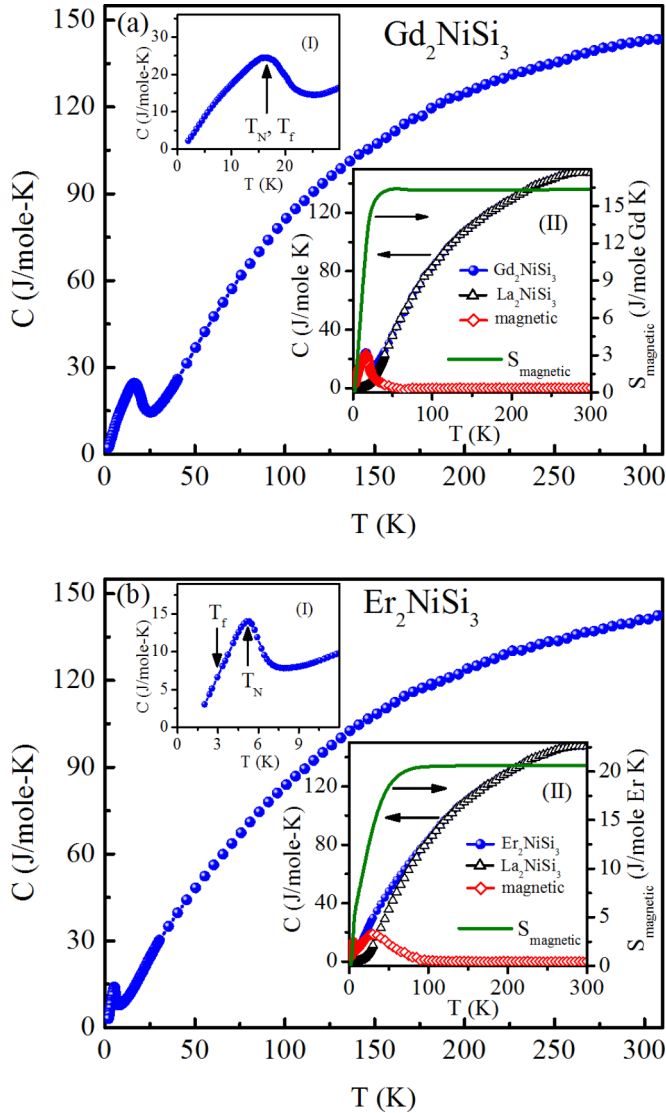
FIG. 12. Zero-field heat capacity of (a) Gd_2NiSi_3 and (b) Er_2NiSi_3. Zero-field heat capacity in an expanded region around the transition temperature is shown in inset I of part (a) for Gd_2NiSi_3 and inset I of part (b) for Er_2NiSi_3. The temperature dependence of zero-field heat capacity of La_2NiSi_3, the magnetic contribution of heat capacity, and the calculated magnetic entropy are plotted in inset II of part (a) for Gd_2NiSi_3 and inset II of part (b) for Er_2NiSi_3.

The magnetic contributions C_{mag} have been calculated by subtracting zero-field heat capacity for isostructural La_2NiSi_3, assuming lattice contributions of the same order of magnitude [inset II, Figs. 12(a) and 12(b)]. The magnetic entropy S_{mag} has been estimated by integrating C_{mag}/T as a function of T. For Gd_2NiSi_3, the magnetic entropy at T_N is $S_{mag} = 12$ J/mol Gd K, which is approximately 70% of the theoretical total magnetic entropy value (17.88 J/mol Gd K). In the case of Er_2NiSi_3, the magnetic entropy at T_N is $S_{mag} = 5.4$ J/mol Er K, which is approximately 23% of the theoretical total magnetic entropy value (23.05 J/mol Er K), and at T_f, $S_{mag} = 3.5$ J/mol Er K, which is approximately 15% of the full moment value. In the case of both compounds, full magnetic entropy is obtained above 50 K, i.e., substantial entropy is contained in the short-range correlations much above their corresponding transition temperatures. The C_{mag} of Er_2NiSi_3 also shows a hump in the high-temperature region (around 30 K), which is a Schottky-type anomaly that occurs due to Zeeman splitting of the $J = 15/2$ level of an Er^{3+} ion. In the case of Gd_2NiSi_3, such an anomaly is absent as there is no crystal-field splitting.

G. Isothermal magnetization and the magnetocaloric effect (MCE)

To investigate the order of the magnetic transition, isothermal magnetization for different temperatures has been measured for both compounds. Figures 13(a) and 13(b) show magnetization as a function of field changes in different temperatures of Gd_2NiSi_3 and Er_2NiSi_3, respectively, for field cycle 0 Oe → 70 kOe → −70 kOe → 70 kOe. No hysteresis can be found in the magnetic isotherms at the lowest temperature (2 K) for both compounds. Figures 13(c) and 13(d) show the field evolution of isothermal magnetization for different temperatures during the field cycle 0 Oe → 70 kOe for the two compounds at much closer intervals of temperatures. According to Banerjee [53], a negative slope in the M^2 versus H/M plot indicates a first-order magnetic phase transition, whereas a positive slope represents a second-order transition. The inset of Figs. 13(a) and 13(b) shows the negative slope of the M^2 versus H/M curve, which suggests the first-order transition in both compounds. Alternatively, it is known that the magnetic free energy $F(M,T)$ according to a Landau expansion can be written as [54]

$$F(M,T) = \frac{C_1(T)}{2}M^2 + \frac{C_3(T)}{4}M^4 + \frac{C_5(T)}{6}M^6 + \cdots - \mu_0 HM, \tag{11}$$

where $C_1(T)$, $C_3(T)$, and $C_5(T)$ are the Landau coefficients, and they can be calculated from the equation

$$\mu_0 H = C_1(T)M + C_3(T)M^3 + C_5(T)M^5. \tag{12}$$

The sign of the coefficient determines the order of transition. If C_3 is negative, the transition is first-order type, and in the case of a second-order transition C_3 is positive. Our best-fitted experimental results show C_3 to be negative for both compounds. This also suggests that the transitions in both compounds are first-order in nature. However, the heat-capacity data do not show a discontinuous jump, which is a characteristic of a first-order phase transition. It may be noted that the heat-capacity measurement has been performed in the absence of any magnetic field. The presence of a magnetic field may perturb the transition process. Moreover, there are instances in which the first derivative of the free energy changes its characteristic nature of sharp discontinuity at the critical temperature in the presence of microscopic random quenched impurities [55]. As the systems studied here also consist of quenched disorders, it may affect the sharpness of the specific-heat curve at the critical temperature. To get a full understanding, and to determine the exact nature of the magnetic transition in such systems, detailed studies are required.

For Gd_2NiSi_3, magnetization increases linearly with magnetic field up to 10 kOe, and after that the magnetization increases rapidly with an applied magnetic field up to 20 kOe.
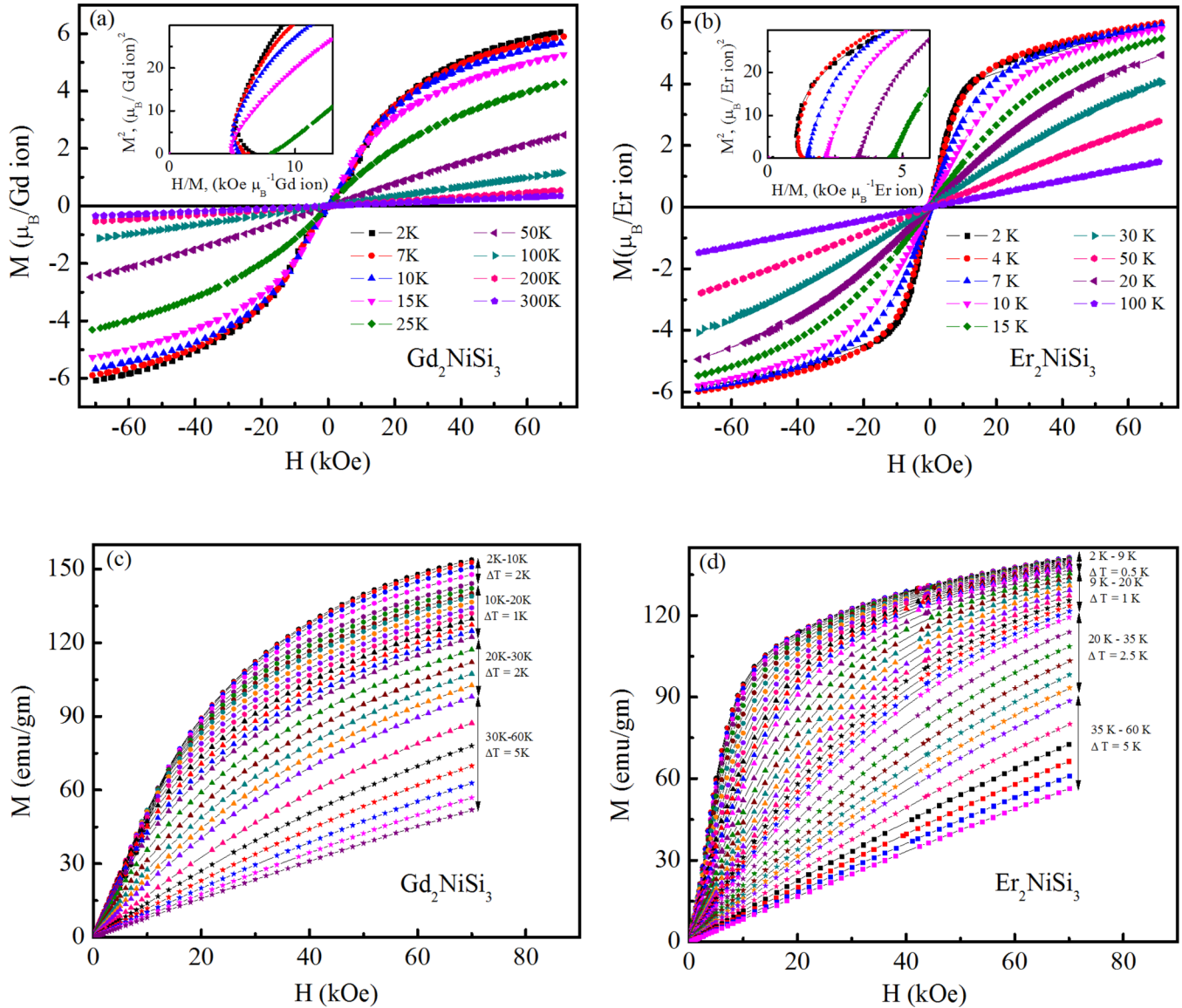
FIG. 13. Isothermal magnetization during field change 0 Oe $\rightarrow$ 70 kOe $\rightarrow$ -70 kOe $\rightarrow$ 70 kOe of (a) Gd$_2$NiSi$_3$ and (b) Er$_2$NiSi$_3$ at different temperatures. Insets show the Arrott plot for the compounds. M-H at different temperatures during a field change 0 Oe $\rightarrow$ 70 kOe of (c) Gd$_2$NiSi$_3$ and (d) Er$_2$NiSi$_3$.

There is a tendency toward moment saturation at fields higher than 20 kOe. In the case of Er$_2$NiSi$_3$, a linear field dependence of magnetization persists up to 5 kOe. In the range 5–10 kOe, magnetization increases rapidly; at fields higher than 10 kOe, magnetic moments exhibit a tendency toward saturation. The values of the magnetic moment at 2 K for a 70 kOe applied field are 6.05 μ_B/Gd^{3+} ion and 6 μ_B/Er^{3+} ion, which are less than the saturation moment value expected for parallel alignment of Gd^{3+} ($gJ = 7\,\mu_B$, with $g = 2$, $J = 7/2$) and Er^{3+} ($gJ = 9\,\mu_B$, with $g = 6/5$, $J = 15/2$) moments. Such a reduced magnetic moment was also observed from the neutron diffraction experiment of Er$_2$NiSi$_3$, and it suggests the frustrated magnetic moments in the systems. At a field strength $H = 20$ kOe for Gd$_2$NiSi$_3$ and 10 kOe for Er$_2$NiSi$_3$, the spin-freezing ground states try to lift their degeneracies and the moments get polarized along the field direction, i.e., metamagnetic-like transitions occur. It was recently predicted

theoretically for such systems with a frustrated ground state that large magnetic entropy changes may be observed at a field strength called the saturation magnetic field [9], where moment values try to saturate.

The values of magnetic entropy change (ΔS_M) have been calculated from magnetization isotherms using the Maxwell thermodynamic relation,

$$\Delta S_M = \int_{H_1}^{H_2} \left(\frac{\partial M}{\partial T} \right) dH. \tag{13}$$

Figures 14(a) and 14(b) show magnetic entropy changes as a function of temperature for different field changes for Gd$_2$NiSi$_3$ and Er$_2$NiSi$_3$, respectively. The maximum values of $-\Delta S_M$ are 18.4 J/kg K for Gd$_2$NiSi$_3$ and 22.6 J/kg K for Er$_2$NiSi$_3$ at a field change of 70 kOe. The values are comparable to or even higher than those of various
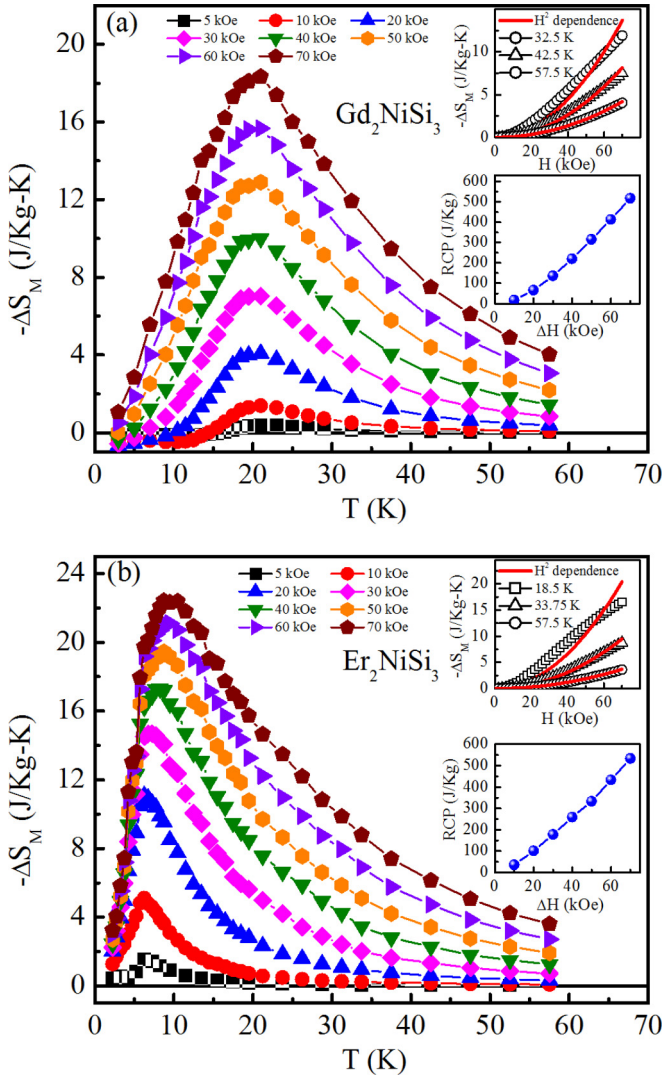
FIG. 14. Temperature dependence of isothermal magnetic entropy change of (a) Gd_2NiSi_3 and (b) Er_2NiSi_3 at different fields. Upper insets show magnetic entropy changes as a function of applied field at different temperatures, along with H^2 dependence. Lower insets show RCP as a function of applied fields.

promising magnetic refrigerant materials in this temperature range [7,8,56–59]. There is no tendency of saturation in $-\Delta S_M$ values even at a strong applied magnetic field strength of 70 kOe. In the low-field region (<5 kOe), $-\Delta S_M$ values are low for both of the compounds. However, large magnetic entropy changes take place at a field $\geqslant 20$ kOe for Gd_2NiSi_3 and at a field $\geqslant 10$ kOe for Er_2NiSi_3. The ΔS_M values are asymmetrically distributed around maximum value, which occurs in the vicinity of magnetic transition temperatures. Generally for systems incorporating a long-range ordering, a symmetric temperature evolution of ΔS_M occurs around the transition temperature. However, asymmetry in ΔS_M has been observed for compounds having spin fluctuations [60] or spin flop transitions [61].

In the paramagnetic region, theoretical calculation predicts $-\Delta S_M \sim H^2/2T^2$, where H is the applied field and T is the corresponding temperature. For both compounds, the best-fitted H^2 dependence is observed for $T > 50$ K [upper insets, Figs. 14(a) and 14(b)], i.e., the true paramagnetic region is well above 50 K, which is consistent with the linear behavior of the inverse susceptibility in the temperature region 60–300 K. In the case of both Gd_2NiSi_3 and Er_2NiSi_3, short-range correlation persists up to a much higher temperature than their respective long-range magnetic ordering temperature, which is responsible for the large change in magnetic entropy over a wide temperature range.

From an application point of view, one of the most important parameters is the relative cooling power (RCP), which determines the amount of heat transfer between the hot and cold reservoirs in an ideal refrigeration cycle. RCP is defined as the product of maximum entropy change (ΔS_M) and full width at half-maximum (δT_{FWHM}) of (ΔS_M) versus T curve. A large value of RCP can be achieved either by getting large ΔS_M or widespread ΔS_M over a large temperature range, or both. The RCP as a function of temperature for different field changes is depicted in the lower insets of Figs. 14(a) and 14(b) for these two compounds. The estimated highest RCP value for Gd_2NiSi_3 is 525 J/kg and for Er_2NiSi_3 it is 540 J/kg for a field change of 70 kOe, which are quite large and comparable to those for most of the reported good refrigerant materials around this temperature range [6,8,56–58,62,63]. Such large values of RCP estimated here have their origin in the asymmetrical spread of ΔS_M over a large temperature range. As mentioned earlier, since the ratio of lattice parameters, c/a, was found to be very close to unity, the magnetic exchange interaction between nearest-neighbor (J_1) and next-nearest-neighbor (J_2) are of comparable strength. The magnetic measurements suggest these to be of opposite sign, which resulted in strong magnetic frustration in these systems. Such frustration is further enhanced as Ni and Si atoms are randomly distributed between the rare-earth ions of consecutive hexagonal planes causing random variation of the conduction electron mediated magnetic RKKY interactions. From the inverse susceptibility and heat-capacity data, we have shown that such short-range magnetic correlation persists up to much higher temperatures than their respective ordering temperatures. The decreasing magnetic entropy over such a wide temperature range is, therefore, most likely to be associated with the presence of magnetic frustration in these systems. In order-to-order transition induced magnetocaloric effects, a large value of ΔS_M is spread over a small temperature region, while in the frustrated systems, e.g., Gd_2NiSi_3 and Er_2NiSi_3, ΔS_M is spread over a broad range of temperature due to spin fluctuation, which makes the relative cooling power much higher. As a result, these two compounds can be used as a magnetic refrigerator over a wide range of temperature, which is very handy for application purposes. Similar to ΔS_M, RCP values also do not show any saturation tendency up to 70 kOe applied field for both of these compounds, and therefore even better performance may be expected if a higher field is used.

Another important parameter for a good refrigerant material is the adiabatic temperature change (ΔT_{ad}), defined as

$$\Delta T_{ad} = [T(S,H) - T(S,0)]_S, \qquad (14)$$

where $T(S,H)$ and $T(S,0)$ are the temperatures at $H_{applied} = H$ and 0, respectively, for a particular entropy S. Temperature
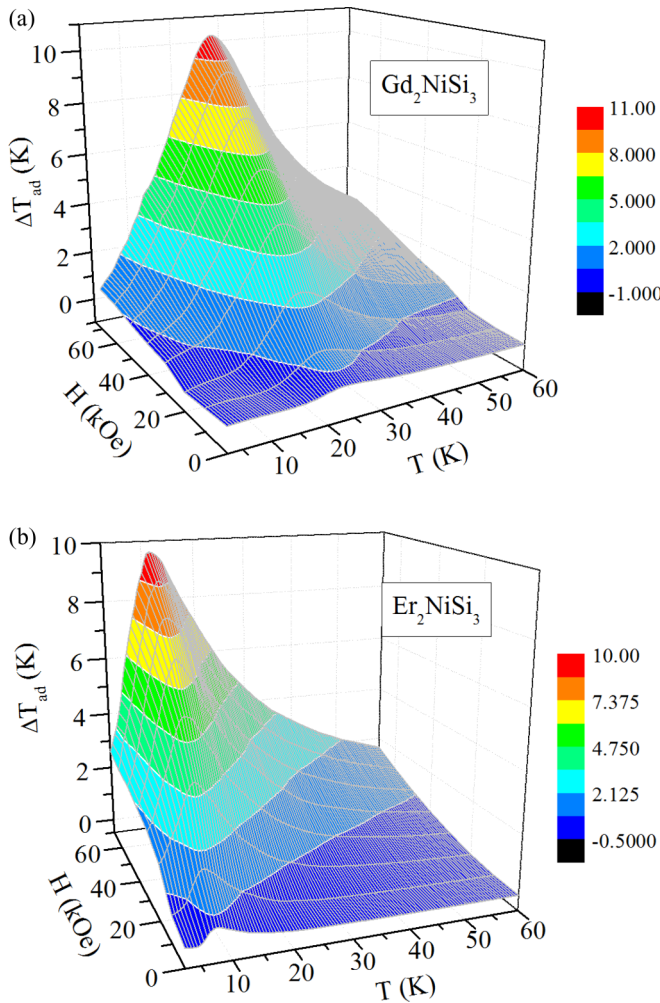
FIG. 15. Temperature dependence of the adiabatic temperature change of (a) Gd_2NiSi_3 and (b) Er_2NiSi_3 for different field changes.

and field evolution of ΔT_{ad} are shown in Figs. 15(a) and 15(b) for Gd_2NiSi_3 and Er_2NiSi_3, respectively. ΔT_{ad} have been calculated using zero-field heat-capacity data [Figs. 12(a) and 12(b)] and ΔS_M for the compounds. As in the case of ΔS_M, here also the peaks broaden asymmetrically around the maximum peak value, which is also attributed to the fluctuation of competing spins over a wide range of temperature. Large values of ΔT_{ad} over a wide range of temperature make the compounds usable over a wide temperature range. The

maximum value of ΔT_{ad} is 9.9 K for Gd_2NiSi_3 and 9.7 K for Er_2NiSi_3, which are significantly large.

H. Summary

We report the successful synthesis of two new stoichiometric compounds Gd_2NiSi_3 and Er_2NiSi_3. These compounds form a single phase in a hexagonal AlB_2-type crystal structure with space group $P6/mmm$. The coexistence of long-range magnetic ordering and magnetically frustrated spin-glass behavior have been confirmed by dc magnetization, ac susceptibility, heat-capacity, and neutron diffraction (for Er_2NiSi_3) measurements. The presence of different magnetic and glassy phases is due to the variation of local environments between the rare-earth ions, inhomogeneously distributed over the sample volume. On the basis of dynamical scaling of ac susceptibility and theoretical analysis of experimentally observed nonequilibrium dynamics, viz., wait-time- and temperature-dependent magnetic relaxation behavior, aging, and memory effects, it is suggested that Gd_2NiSi_3 is a canonical spin-glass material, whereas Er_2NiSi_3 is a reentrant spin cluster-glass material. In the case of Gd_2NiSi_3, spin-freezing temperature coincides with long-range antiferromagnetic ordering temperature, $T_f = T_N \sim 16.4$ K. In contrast, Er_2NiSi_3 undergoes antiferromagnetic ordering below 5.4 K (T_N), while spin freezing occurs below 3 K (T_f). The large magnetocaloric effect has been observed over a wide temperature range due to spin fluctuation over a wide range of temperature much above their respective peak temperatures. Experimentally observed large values of MCE (large $-\Delta S_M$, large RCP, and large ΔT_{ad} simultaneously) for these two magnetically frustrated compounds are in agreement with the theoretical predictions. Gd_2NiSi_3 and Er_2NiSi_3 are in that rare category in which a large MCE emerges due to the frustrated magnetic ground state.

[1] K. A. Gschneidner and V. K. Pecharsky, Annu. Rev. Mater. Sci. **30**, 387 (2000).

[2] K. A. Gschneidner, Jr., V. K. Pecharsky, and A. O. Tsokol, Rep. Prog. Phys. **68**, 1479 (2005).

[3] V. K. Pecharsky and K. A. Gschneidner, Jr., Phys. Rev. Lett. **78**, 4494 (1997).

[4] O. Tegus, E. Brück, K. H. J. Buschow, and F. R. de Boer, Nature (London) **415**, 150 (2002).

[5] V. Provenzano, A. J. Shapiro, and R. D. Shull, Nature (London) **429**, 853 (2004).

[6] L. Li, K. Nishimura, W. D. Hutchison, Z. Qian, D. Huo, and T. Namiki, Appl. Phys. Lett. **100**, 152403 (2012).

[7] T. Samanta, I. Das, and S. Banerjee, Appl. Phys. Lett. **91**, 152506 (2007).

[8] W. J. Hu, J. Du, B. Li, Q. Zhang, and Z. G. Zhang, Appl. Phys. Lett. **92**, 192505 (2008).

[9] M. E. Zhitomirsky, Phys. Rev. B **67**, 104421 (2003).

[10] M. E. Zhitomirsky and H. Tsunetsugu, Phys. Rev. B **70**, 100403(R) (2004).

[11] B. Schmidt, P. Thalmeier, and N. Shannon, Phys. Rev. B **76**, 125113 (2007).

[12] S. S. Sosin, L. A. Prozorova, A. I. Smirnov, A. I. Golov, I. B. Berkutov, O. A. Petrenko, G. Balakrishnan, and M. E. Zhitomirsky, Phys. Rev. B **71**, 094413 (2005).

[13] J. W. Sharples, D. Collison, E. J. L. Mclnnes, J. Schnack, E. Palacios, and M. Evangelisti, Nat. Commun. **5**, 5321 (2014).

[14] R. A. Gordon, C. J. Warren, M. G. Alexander, F. J. DiSalvo, and R. Pöttgen, J. Alloys Compd. **248**, 24 (1997).

[15] A. P. Ramirez, in *Handbook of Magnetic Materials*, edited by K. H. J. Buschow (Elsevier, Amsterdam, 2001), Vol. 13, Chap. 4.

[16] S. F. Edwards and P. W. Anderson, J. Phys. F **5**, 965 (1975); Y. Crespo, A. Andreanov, and N. Seriani, Phys. Rev. B **88**, 014202 (2013).

[17] D. Huo, J. Sakurai, T. Kuwai, Y. Isikawa, and Q. Lu, Phys. Rev. B **64**, 224405 (2001).

[18] J. A. Mydosh, *Spin Glasses: An Experimental Introduction* (Taylor & Francis, London, 1993), Chap. 3.

[19] D. X. Li, S. Nimori, Y. Shiokawa, Y. Haga, E. Yamamoto, and Y. Onuki, Phys. Rev. B **68**, 012413 (2003).

[20] D. Li, X. Zhao, and S. Nimori, J. Phys.: Condens. Matter **21**, 026006 (2009).

[21] C. Tien, C. H. Feng, C. S. Wur, and J. J. Lu, Phys. Rev. B **61**, 12151 (2000).

[22] S. Majumdar, E. V. Sampathkumaran, M. Brando, J. Hemberger, and A. Loidl, J. Magn. Magn. Mater. **236**, 99 (2001).

[23] M. Szlawska and D. Kaczorowski, Phys. Rev. B **84**, 094430 (2011).

[24] M. Szlawska and D. Kaczorowski, Phys. Rev. B **85**, 134423 (2012).

[25] J. Rodríguez-Carvajal, Physica B **192**, 55 (1993).

[26] K. Binder and A. P. Young, Rev. Mod. Phys. **58**, 801 (1986).

[27] M. Gabay and G. Toulouse, Phys. Rev. Lett. **47**, 201 (1981).

[28] J. R. L. de Almeida and D. J. Thouless, J. Phys. A **11**, 983 (1978).

[29] S. Chatterjee and A. K. Nigam, Phys. Rev. B **66**, 104403 (2002).

[30] J. Lago, S. J. Blundell, A. Eguia, M. Jansen, and T. Rojo, Phys. Rev. B **86**, 064412 (2012).

[31] S. Ghara, B.-G. Jeon, K. Yoo, K. H. Kim, and A. Sundaresan, Phys. Rev. B **90**, 024413 (2014).

[32] P. C. Hohenberg and B. I. Halperin, Rev. Mod. Phys. **49**, 435 (1977).

[33] T. Mori and H. Mamiya, Phys. Rev. B **68**, 214422 (2003).

[34] J. Souletie and J. L. Tholence, Phys. Rev. B **32**, 516(R) (1985).

[35] A. Bhattacharyya, S. Giri, and S. Majumdar, Phys. Rev. B **83**, 134427 (2011).

[36] D. Chu, G. G. Kenning, and R. Orbach, Phys. Rev. Lett. **72**, 3270 (1994).

[37] S. Sahoo, O. Petracic, W. Kleemann, P. Nordblad, S. Cardoso, and P. P. Freitas, Phys. Rev. B **67**, 214422 (2003).

[38] R. Mathieu, P. Jönsson, D. N. H. Nam, and P. Nordblad, Phys. Rev. B **63**, 092401 (2001).

[39] Y. Sun, M. B. Salamon, K. Garnier, and R. S. Averback, Phys. Rev. Lett. **91**, 167206 (2003).

[40] K. Jonason, E. Vincent, J. Hammann, J. P. Bouchaud, and P. Nordblad, Phys. Rev. Lett. **81**, 3243 (1998).

[41] M. Sasaki, P. E. Jönsson, H. Takayama, and H. Mamiya, Phys. Rev. B **71**, 104405 (2005).

[42] D. S. Fisher and D. A. Huse, Phys. Rev. B **38**, 373 (1988); **38**, 386 (1988).

[43] W. L. Mcmillan, J. Phys. C **17**, 3179 (1984).

[44] V. S. Dotsenko, J. Phys. C **18**, 6023 (1985).

[45] E. Vincent, J. Hammann, M. Ocio, J. P. Bouchaud, and L. F. Cugliandolo, in *Complex Behaviour of Glassy Systems*, edited by E. Rubi (Springer, Berlin, 1996).

[46] M. Ulrich, J. García-Otero, J. Rivas, and A. Bunde, Phys. Rev. B **67**, 024416 (2003).

[47] K. Tomiyasu, J. Fukunaga, and H. Suzuki, Phys. Rev. B **70**, 214434 (2004).

[48] D. Fiorani, S. Viticoli, J. L. Dormann, J. L. Tholence, and A. P. Murani, Phys. Rev. B **30**, 2776 (1984).

[49] J. N. Reimers, Phys. Rev. B **46**, 193 (1992).

[50] Y. M. Jana, O. Sakai, R. Higashinaka, H. Fukazawa, Y. Maeno, P. Dasgupta, and D. Ghosh, Phys. Rev. B **68**, 174413 (2003).

[51] V. K. Anand, D. T. Adroja, A. D. Hillier, J. Taylor, and G. André, Phys. Rev. B **84**, 064440 (2011).

[52] J. A. Blanco, D. Gignoux, and D. Schmitt, Phys. Rev. B **43**, 13145 (1991).

[53] S. K. Banerjee, Phys. Lett. **12**, 16 (1964).

[54] X. B. Liu and Z. Altounian, J. Magn. Magn. Mater. **292**, 83 (2005).

[55] Y. Imry and M. Wortis, Phys. Rev. B **19**, 3580 (1979).

[56] S. Gupta, R. Rawat, and K. G. Suresh, Appl. Phys. Lett. **105**, 012403 (2014).

[57] L. M. da, Silva, A. O. dos Santos, A. A. Coelho, and L. P. Cardoso, Appl. Phys. Lett. **103**, 162413 (2013).

[58] Z. J. Mo, J. Shen, X. Q. Gao, Y. Liu, C. C. Tang, J. F. Wu, F. X. Hu, J. R. Sun, and B. G. Shen, J. Alloys Compd. **626**, 145 (2015).

[59] A. O. Pecharsky, Y. Mozharivskyj, K. W. Dennis, K. A. Gschneidner, Jr., R. W. McCallum, G. J. Miller, and V. K. Pecharsky, Phys. Rev. B **68**, 134452 (2003).

[60] A. M. Tishin and Y. I. Spichkin, *The Magnetocaloric Effect and Its Applications* (IOP, New York, 2003).

[61] O. Toulemonde, P. Roussel, O. Isnard, G. André, and O. Mentré, Chem. Mater. **22**, 3807 (2010).

[62] J. Chen, B. G. Shen, Q. Y. Dong, F. X. Hu, and J. R. Sun, Appl. Phys. Lett. **96**, 152501 (2010).

[63] H. Zhang, B. G. Shen, Z. Y. Xu, J. Shen, F. X. Hu, J. R. Sun, and Y. Long, Appl. Phys. Lett. **102**, 092401 (2013).